PERGAMON

Aerosol Science 32 (2001) 993–1008

Journal of
Aerosol Science

www.elsevier.com/locate/jaerosci

Characterization of the aerosols resulting from arc welding processes

Anthony T. Zimmer[a,*], Pratim Biswas[b]

[a]*Division of Applied Research and Technology, National Institute for Occupational Safety and Health, 4676 Columbia Parkway, Cincinnati, OH 45226, USA*
[b]*Departments of Chemical and Civil Engineering, Washington University, One Brookings Drive, Campus Box 1180, St. Louis, MO 63130-4899, USA*

Received 8 August 2000; received in revised form 30 November 2000; accepted 12 December 2000

Abstract

As a result of recent research on the potentially adverse health effects of sub-micrometer aerosols, a generation chamber and sampling system was designed to characterize aerosols from a popular welding system that utilized either gas metal arc welding or flux cored arc welding techniques. The experimental apparatus allowed flexibility in changing arc welding parameters, sample locations, and was designed to promote the steady-state generation of fumes over several minutes. In contrast to prior studies where the particle size distribution was weighted by mass without regard to its time/temperature history, the welding aerosols in this study were temporally collected and weighted by a lower moment, particle number. The results demonstrated that the welding alloy had a marked effect on the particle size distribution, morphology and chemical aspects of the resultant fume. In addition, the particle size distributions from these processes were multi-modal and dynamically changed with time.

Keywords: Welding; Fumes; Arc

1. Introduction

Welding operations produce gaseous and aerosol by-products composed of a complex array of metals, metal oxides, and other chemical species volatilized from either the base metal, the welding electrode, or the flux material. These processes generate fumes on the order of 100–400 mg m^{-3} in the rising column of heated air directly above the arc. Average breathing zone concentration

* Corresponding author. Tel.: + 1-513-841-4370; fax: + 1-513-841-4500.
E-mail address: atz0@cdc.gov (A. T. Zimmer).

0021-8502/01/$ - see front matter
PII: S0021-8502(01)00035-0

depends to a great extent on the welding process used, but levels of 5 $mg\,m^3$ are typical throughout the industry (Ulfvarson, 1981). Census data indicates that over 600,000 workers in the United States are involved in welding or allied processes. Animal and epidemiological studies suggest that welding is associated with a wide range of adverse health effects such as metal fume fever, pneumonitis, chronic bronchitis, and decrements in pulmonary function (NIOSH, 1988). Welding processes are known to generate sub-micrometer sized aerosols, and recent research has indicated sub-micrometer aerosols may cause adverse health effects due to their size (Ferin, Oberdorster, Penney, & Soderholm, 1990; Gilmour, Brown, Beswick, & Benton, 1997; Oberdorster et al., 1990; Takenaka, Dornhofer-Takenaka, & Muhle, 1986).

Previous studies have examined welding fumes that were generally based upon techniques recommended by the American Welding Society and the American National Standards Institute. A test chamber was used to draw air through a filter pad to collect welding process fumes. The fume formation rate (FFR) (mass of aerosol collected per unit time) was frequently used to characterize the relative "cleanliness" of a welding process (Heile & Hill, 1975; Hilton & Plumridge, 1991; Thornton & Stares, 1994). Parameters such as the welding alloy, arc voltage, and electrode extension were typically varied to determine their effect on the FFR. For example, the FFRs for gas metal arc welding (GMAW) processes varied from 0.035 to 0.37 $g\ min^{-1}$ depending upon the alloy selected and the arc voltage (Heile & Hill, 1975). GMAW processes, frequently encountered in the welding industry, use welding alloys that require shield gases (e.g., argon/carbon dioxide) to protect metals within the arc and to provide the desired arc characteristics (Fig. 1). In contrast, flux cored arc welding (FCAW) processes had higher FFRs with values ranging from 0.75 to 2.5 $g\ min^{-1}$ (Heile & Hill, 1975). The metallurgy of FCAW alloys are different from GMAW alloys in that they incorporate fluxing compounds within the core of the welding wire to fully or partially shield the arc welding process.

Several other analytical techniques have been used to characterize arc welding processes including particle size distribution using cascade impaction (Heile & Hill, 1975; Hewett, 1995), particle morphology using transmission electron microscopy (Fasiska, Nasta, & Scan, 1982; Hewitt & Gray, 1983), and the chemistry of the bulk fume (Fasiska et al., 1982; Heile & Hill, 1975; Hewitt & Gray, 1983) and individual particles (Fasiska et al., 1982; Tandon et al., 1985; Voitkevich, 1988). The aerosols produced from GMAW and FCAW differ markedly. The aerosols from GMAW processes are almost entirely sub-micrometer (Heile & Hill, 1975; Hewett, 1995) and are smaller than that of FCAW (Heile & Hill, 1975). The aerosols generated from GMAW processes resulted in chain-like structures composed primarily of magnetite ($\gamma\,Fe_3O_4$) (Hewitt & Gray, 1983). In contrast, the particle morphology of aerosols generated from FCAW processes was more complex, resulting in the formation of both chainlike and spherical structures composed of transition and alkali metals (Kalliomaki, Grekula, Hagberg, & Sivonen, 1987).

Prior studies have focused primarily upon characterizing aerosols based upon the mass of the aerosol (i.e., fume formation rates and cascade impaction techniques) as the current standards for welding fumes are weight based. However, this may not be adequate if the toxicologically significant parameter is a lower moment of the particle size distribution such as particle number or particle surface area. Additionally, prior research has focused upon collecting and characterizing the welding process aerosol without regard to the time–temperature history of the aerosol. The arc welding aerosol is similar to a combustion aerosol (Lin & Biswas, 1994) and will be significantly altered with respect to where it is sampled. The following presents experimental results to

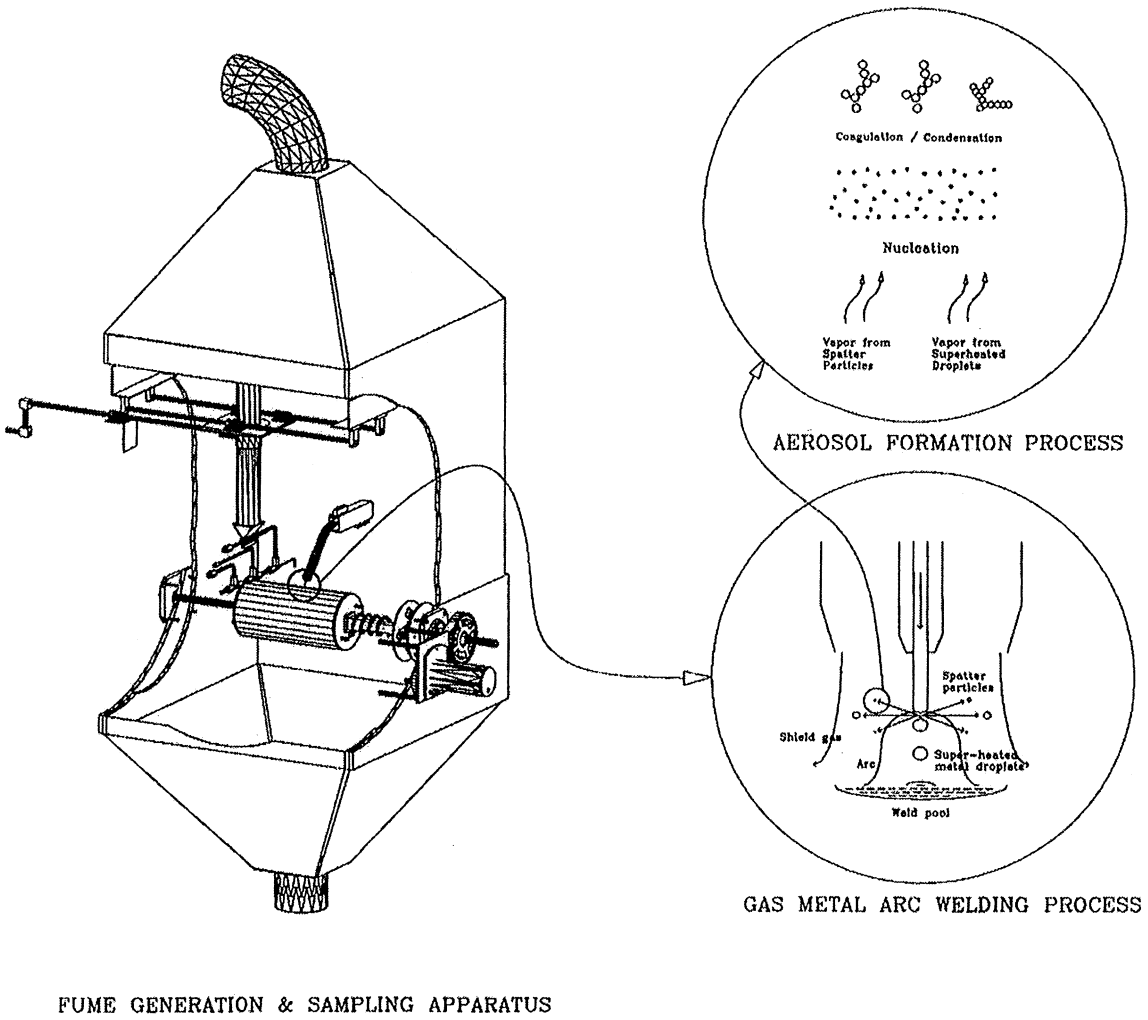

Fig. 1. Schematic illustrating: (1) the fume generation and sampling apparatus, (2) the operation of a gas metal arc welding (GMAW) process, and (3) the probable formation of aerosols during a GMAW process.

characterize welding aerosols produced from this apparatus and includes: (1) the spatial and temporal variations of particle number concentration within the fume chamber, (2) the effect of welding alloy on the chemistry, morphology and particle number size distribution, and (3) the temporal variation of the particle number size distribution.

2. Experimental

The experimental apparatus used to study the arc welding fume was designed to allow for flexibility in changing arc welding parameters and sample locations; and to promote the steady-state generation of fumes over a period of several minutes (Fig. 1). A high quality, commercial arc

welding system (Miller Deltaweld Series 452 power source and Miller S-62 wire feeder) was selected to generate the welding fumes. This system can be readily configured to weld using two popular processes, GMAW or FCAW, depending upon the wire alloy selected. The welding gun was placed within a sealed stainless-steel chamber (121 cm height, 91 cm length, 81 cm width) and welding was performed on a rotating metal cylinder. In this setup, wire alloy, fed at a constant speed, provided the filler material for the arc welding process. Within the high temperature regime of the arc, the solid wire transformed into superheated liquid metal droplets that deposited onto a mild steel cylindrical substrate (16.8 cm diameter, 0.66 cm thickness, ASTM A-53-B grade steel) (Fig. 1). A low speed motor, located outside of the chamber, was used to rotate the cylinder at constant speed of 38 cm min^{-1}. The thread pitch of the Acme screw determined the distance between the overlapping weld bead (0.25 cm). Depending on the welding process selected, shield gases were used to stabilize the arc and to prevent chemical oxidation of the molten metal droplets and molten substrate. The shield gases, composed of argon and carbon dioxide, were metered to the welding unit using mass flow controllers (Unit Instruments Inc., Orange, CA, Model UFC-1100). This allowed flexibility in controlling the shield gas flowrate and composition. Metal fumes were generated from an arc welding process directly from volatilization of the metal vapor from the superheated molten droplets, and indirectly from spatter particles ejected during the welding process (Gray & Hewitt, 1982) (Fig. 1). HEPA-filtered, particle-free air was pulled up vertically through the chamber using an industrial air cleaner (ACE Corp, Model 73-800G). Honeycomb flow-straighteners were used to smooth the air prior to reaching the cylindrical substrate. The fume laden air was filtered, using 95% efficiency filters, prior to being exhausted to the outside. When configured as a flow-through system, this apparatus simulated exhausting welding fumes using an industrial ventilation system. This apparatus can also be operated as a stagnant chamber, a configuration that simulated welding without an engineering control.

The welding process generated an aerosol-laden plume that mixed with the HEPA filtered air. A movable sampling probe was used to collect fume samples for aerosol measurements (Fig. 1). The probe, a modified design from Biswas, Li, and Pratsinis (1989), allowed for accurate sample collection in both the horizontal and vertical directions relative to the arc location. Cylindrical symmetry, about a vertical axis centered on the weld site was assumed. Samples were collected isoaxially, although not isokinetically. Due to the small Stokes number of welding aerosols (< 0.01), isokinetic losses are expected to be negligible (Hinds, 1999). Because of the high number concentrations encountered during this process, a dual-stage dilution system was designed to allow up to a 1000-fold decrease in the particle number concentration (Fig. 2). This design served to quench chemical and aerosol dynamic processes within the sample line to allow collection of representative samples. The sample probe was modified to significantly reduce the time for second stage dilution to a millisecond timescale.

Following dilution, aerosol measurements were taken by directing a portion of the diluted sample to a condensation particle counter (CPC) (TSI Inc., Model 3022A) or a scanning mobility particle sizer (SMPS) (TSI Inc., an Electrostatic Classifier, Model 3080, using either a long differential mobility analyzer (DMA), Model 3081 or a nano differential mobility analyzer, Model 3085, and a condensation particle counter, model 3022A operated in the scanning mode). The CPC was used to measure particle number concentration in real-time, and the SMPS was used to measure the particle number size distribution of aerosols. The SMPS required approximately two minutes to measure a particle size distribution in the nanometer size regime. To evaluate the effect

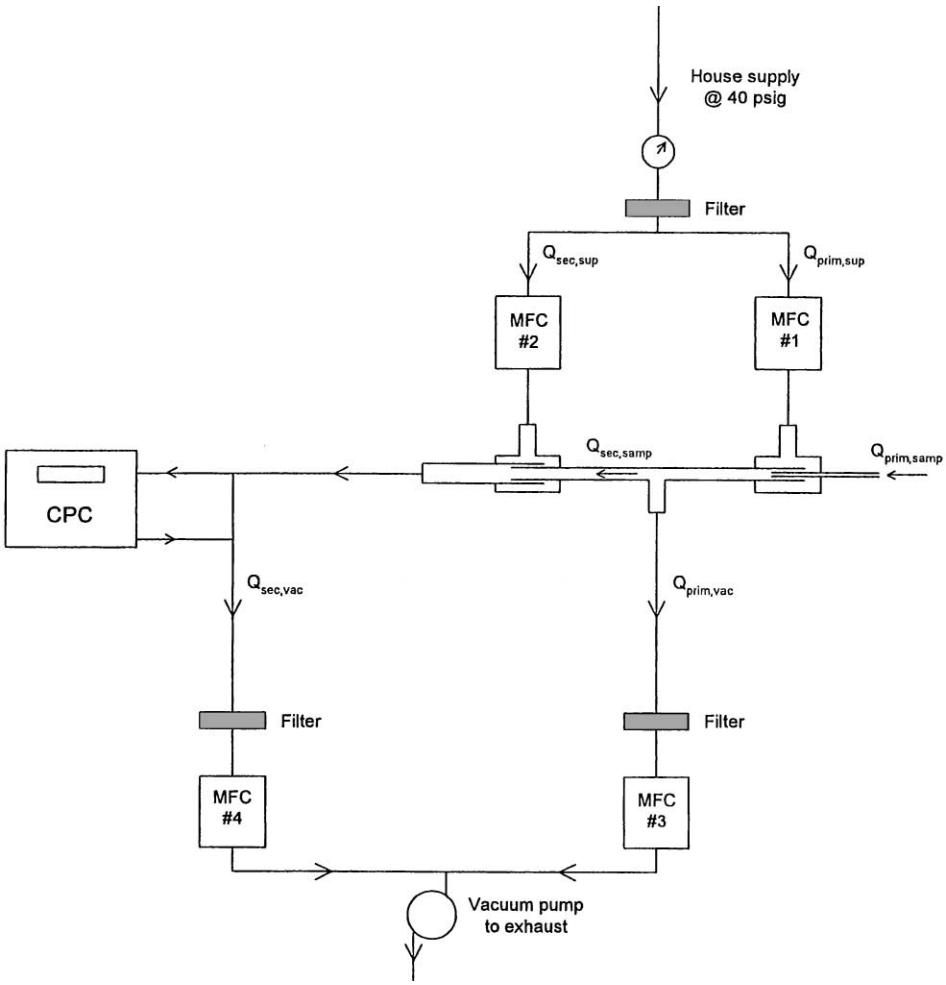

Fig. 2. Dual-stage dilution system to collect welding aerosols (note: MFC is mass flow controller, and CPC is condensation particle counter).

of temporal variation on the SMPS measurements, the CPC was first used to characterize the spatial and temporal variations of the aerosol at a fixed vertical/horizontal locations within the fume generation chamber. In addition, the elemental composition and morphology of the fume was characterized by transmission electron microscopy (TEM) (Philips, Model 420), coupled with energy dispersive X-ray analysis (EDAX, Princeton Gamma-tech Avalon, Model 4000), to determine the elemental composition of the particles. Fume samples were collected at specific residence times by directly collecting aerosols onto a TEM grid using a cold finger technique. This technique involved securing the TEM grid onto a heat sink (i.e., brass grid holder). By attaching the holder to the sample probe (Fig. 1), aerosols were thermophoretically collected onto the grid by moving the apparatus into and out of the welding plume.

The flexibility of this experimental apparatus allowed for ease in changing various welding generation and sampling conditions such as: the welding alloy type/feed-rate, the welding substrate

composition, the welding voltage, the extension height (distance between the arc welding gun and the substrate), the shield gas composition/flowrate, the average chamber velocity, and the aerosol sample dilution ratio. Conditions that were held constant in this work include: the wire feed speed (965 cm min^{-1}), the distance between the arc welding gun and the substrate (1 cm), the welding substrate, designated as ASTM A-53-B grade steel (linear travel speed of 38 cm min^{-1}), the arc welding voltage (20.5 V) and the arc amperage (allowed to float between 195 and 205 A).

3. Results and discussion

3.1. Spatial and temporal variations of particle number concentration

To characterize the behavior of the fume generation apparatus both spatially and temporally, CPC measurements were taken over a 225 s interval at fixed horizontal and vertical positions. During these experiments, the following conditions (in addition to the items mentioned in the previous section) were held constant: the GMAW wire alloy (designated as ER70S-6, with a diameter of 0.089 cm), the volumetric flowrate and composition of the shield gas (18 lpm, 90% argon and 10% carbon dioxide), and the volumetric flowrate of the HEPA filtered, flow straightened air moving through the fume generation chamber (2725 lpm with an average velocity of 366 cm min^{-1}). Horizontal measurements were taken at 0, 5, 10, and 15 cm intervals, measured from the arc centerline. Vertical measurements were taken at 4.8, 9.6, 14.4, and 19.2 cm intervals, measured from the substrate surface. Sixteen points were sampled, although replicate measurements were taken at several locations to insure the reproducibility of the sample results. In all cases, the dilution system was set to reduce the number concentration of the aerosol entering the probe by 1000-fold.

Fig. 3 illustrates the variation of particle number concentration over a 50 s time interval (125–175 s after the start of the sample run with measurements taken at 1 s intervals along the arc centerline). As the measurement height increased from the arc welding process, the number concentration decreased. The average number concentration decreased from 1.42×10^7 particles cm^{-3} at a height of 4.8 cm to 3.67×10^6 particles cm^{-3} at a height of 19.2 cm. This four-fold decrease can be mainly attributed to the dilution of the welding fume by the surrounding HEPA filtered air and to coagulation of the fume particles. The number concentration fluctuates close to the arc, and this is dampened as the distance from the arc increases. For example, at a distance of 4.8 cm, the coefficient of variation (standard deviation divided by the average number concentration) was 0.25. At a height of 19.2 cm, the coefficient of variation decreased to 0.047. This is reasonable in that the high arc temperatures and shield gases surrounding the arc create instability and local turbulence, resulting in the fluctuations observed using the CPC.

Fig. 4a–d illustrates how the average particle number concentration varied over four time intervals with respect to the horizontal and vertical position from the arc welding process. These values represent arithmetic averages over the fifty second interval evaluated. For all of the time intervals in question, an increase in vertical and horizontal distance away from the arc resulted in a decrease in the average particle number concentration. This is a reasonable finding because the highest particle concentrations would be expected near the arc. In Fig. 4a, the average number concentration varied from 1.6×10^7 particles cm^{-3} near the arc (0 cm horizontal, 4.8 cm vertical)

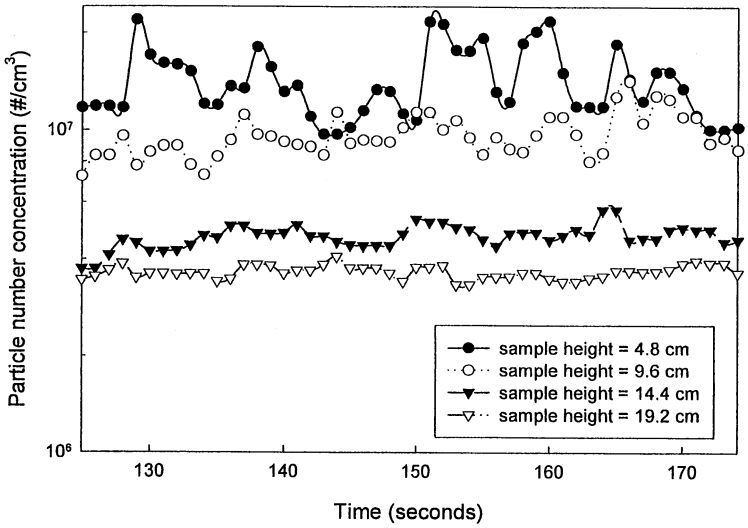

Fig. 3. Condensation particle counter results for a 50 seconds period (125–175 s after the start of the sample run) with measurements taken horizontally along the arc centerline (note: measurements taken at one second intervals).

to 3.2×10^6 particles cm^{-3} at the point corresponding to the farthest point measured (15 cm horizontal, 19.2 cm vertical). It is interesting to note that as the time interval increased, the average number concentration increased at locations well away from the arc welding process (Fig. 4b–d). For example, the average particle number concentration increased from 3.2×10^6 particles cm^{-3} during the first time interval (25–75 s) to 5.1×10^6 particles cm^{-3} during the last time interval (175–225 s) at the sample location most distant from the arc (15 cm horizontal, 19.2 cm vertical). This slight, but reproducible increase may be attributed to the heating of the cylindrical substrate. Temperature measurements taken slightly above the surface of the substrate during a welding run revealed that the temperature increased from 21 to 264°C during the sample run. The energy produced during the welding process heated the cylindrical substrate, resulting in a buoyant thermal plume that increased the dispersion of the welding fume. As a result, the average number concentration slightly increased over time at sample locations away from the arc welding process.

3.2. *Effect of welding alloy on the chemistry, morphology and particle number size distribution*

The welding fumes generated from two distinctly different welding processes were investigated: gas metal arc welding and flux cored arc welding. The gas metal alloy, designated as ER70S-6, was used with a shield gas composed of 90% argon and 10% carbon dioxide. According to the material safety data sheet provided by the manufacturer, this alloy is composed of the following elements by weight: 97.5% iron, 1.2–1.6% manganese, 0.8–1.0 silica, and 0.1% copper. The flux cored alloy, designated as E71T-11, was used without a shield gas. The metal alloy surrounding the flux core contains roughly the same ingredients as the GMAW alloy. The flux core ingredients are proprietary, but often contain alkali metals and fluoride to protect the arc welding alloys. HEPA-filtered, flow-straightened air moved through the fume generation chamber with an average

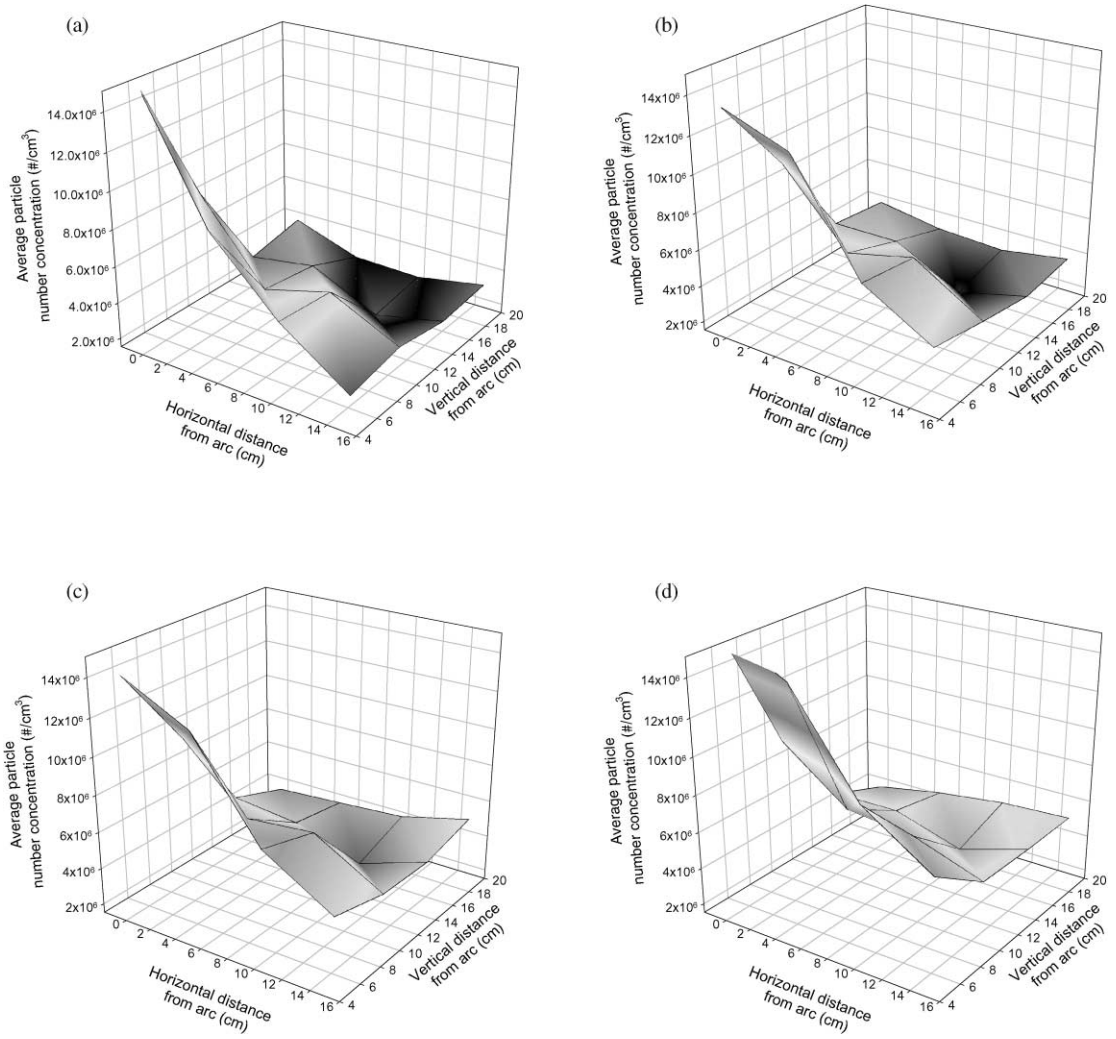

Fig. 4. Condensation particle counter results for time intervals corresponding to (a) 25–75 s, (b) 75–125 s, (c) 125–175 s, and (d) 175–225 s (note: the average particle number concentration is linearly scaled).

velocity of 366 cm min^{-1} (volumetric flowrate of 2725 lpm). Measurements were collected on the arc centerline at a vertical distance of 19.2 cm with a corresponding residence of approximately 3.2 s (i.e., time for a parcel of air to travel from the arc to the sample probe). The dilution system was set to reduce the number concentration of the aerosol entering the probe by 150-fold.

Fig. 5 shows the particle number size distributions obtained from the two alloys using the SMPS configured with the Long DMA (16.5 nm $< d_{\mathrm{p}} <$ 562 nm). Three replicate samples were collected for each alloy and the bars represent the standard error associated with each particle size bin. As seen in Fig. 5, the aerosols generated from the GMAW alloy were smaller than that of the FCAW alloy (count median particle diameters of 149 and 352 nm, respectively). Although the particle number concentration of the GMAW alloy (5.72×10^6 # cm^{-3}) was slightly higher than that of

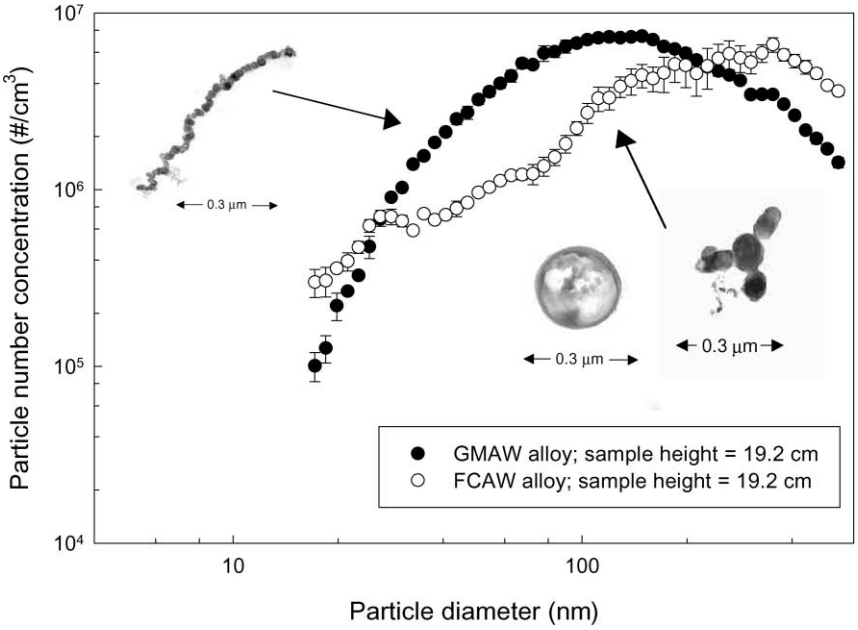

Fig. 5. Scanning mobility particle sizer results at a sample height of 19.2 cm above the arc centerline using a gas metal arc welding (GMAW) alloy and a flux cored arc welding (FCAW) alloy; and TEM images of representative aerosols from each welding process (note: a Long DMA was used with 16.5 nm $< d_p <$ 562 nm).

the FCAW alloy (4.24×10^6 # cm^{-3}), the upper limit of the SMPS did not adequately reveal the right hand side of the both distributions, especially when viewing the FCAW alloy results. These results were consistent with previous studies when comparing FFRs and particle sizing from these welding processes (Heile & Hill, 1975).

Another observation that is apparent from Fig. 5 is the difference in the appearance of the particle size distributions. At this height, the distribution for the GMAW alloy appears unimodal and much smoother than that of the FCAW alloy which appears coarse and potentially multi-modal. When comparing the metallurgy of both processes, GMAW is less complex than that of FCAW. GMAW alloys are composed primarily of iron (97–98%) and rely on the use of shield gases to protect the metal droplets from oxidation. In contrast, the FCAW alloy use ingredients contained within the core of the alloy to protect the metal droplets contained within the arc. The complex metallurgical chemistry of the FCAW process affects the dynamic mechanisms involved in forming an aerosol and could be responsible for the multi-modal behavior that was experimentally observed (Fig. 5). TEM samples of both processes tends to support this view in that the GMAW aerosols are homogeneous, especially, when compared to the FCAW aerosols (Fig. 5). The aerosols generated from the GMAW alloy were composed primarily of homogeneous chain-like agglomerates (Fig. 5). According to the EDAX analysis, the agglomerates were composed of iron, manganese, and silica. It appears that the dominant aerosol formation mechanisms during this process include nucleation of primary particles, followed by growth through coagulation. The chainlike nature of the aerosols generated by this process is probably related to the formation of primary

particles composed primarily of magnetite (γFe_3O_4) with magnetic forces dictating the simple linear structure of the agglomerates. In contrast, the aerosols generated from the FCAW alloy are more complex and contain a mixture of chainlike and spherical structures (Fig. 5). This finding suggests that nucleation of primary particles, composed primarily of magnetite, is followed by competing dynamic mechanisms including growth by coagulation and condensation of lighter elements found in the flux core. EDAX analysis of the FCAW aerosols supports this finding in revealing the presence of elements found in the GMAW process, as well as alkali metals such as magnesium, calcium, and barium. These findings were consistent with prior studies (Hewitt & Gray, 1983; Kalliomaki et al., 1987).

3.3. Temporal variations in particle number size distribution

Having characterized the temporal and spatial variations of the particle number concentration within the fume chamber, particle number size distribution measurements were used to determine the temporal evolution of the welding aerosol. During these experiments, the following conditions were held constant: the GMAW wire alloy (designated as ER70S-6, with a diameter of 0.089 cm), the volumetric flowrate and composition of the shield gas (18 lpm, 90% argon and 10% carbon dioxide), and the volumetric flowrate of the HEPA filtered, flow straightened air moving through the fume generation chamber (2725 lpm with a average velocity of 366 cm min^{-1}). During these experiments, the dilution system was set to reduce the number concentration of the aerosol entering the probe by 150-fold.

Fig. 6a–c shows the particle number size distributions obtained from a GMAW alloy at three sample heights corresponding to increasing residence times. Three replicate samples were collected at each sample height and the bars represent the standard error associated with each particle bin. At each sample height, the SMPS was configured both with the Nano DMA ($4.53\ nm < d_p < 153\ nm$) and Long DMA ($16.5 < d_p < 562\ nm$). Several general observations are apparent from Fig. 6a–c. The replicate samples for each location and each DMA appear reproducible, although the standard error increases as the particle diameter decreases. This is reasonable in that the particle counting efficiency decreases with decreasing particle size. The results for both the nano and long DMA appear to qualitatively agree with one another, although the long DMA results appear to be distinctly smoother. Several factors could contribute to the differences noted between the results obtained using the nano and long DMAs. One reason could relate to the physical differences between the DMAs in that geometry of the nano DMA was optimized to minimize diffusional losses while the long DMA was designed to characterize particles over a broad size range. Another reason could relate to the chainlike nature of the GMAW aerosol (Fig. 5) in that particles may be charged in a slightly different manner within each DMA. Finally, as the sample height increases (with a corresponding increase in residence time), the number concentration of small diameter particles appears to markedly decrease. This is reasonable in that smaller particles are scavenged by larger particles through coagulation.

Several specific observations can also be made at each sample height. The size distribution at a vertical height of 4.8 cm (corresponding to a residence time of 0.8 s), along the arc centerline appears to be multi-modal with good reproducibility (Fig. 6a). In the overlap regions for the nano and long DMA, a mode appears to be evident for both instruments at a particle size of approximately 60 nm. For both DMAs, other modes are possible, however, they do not appear to

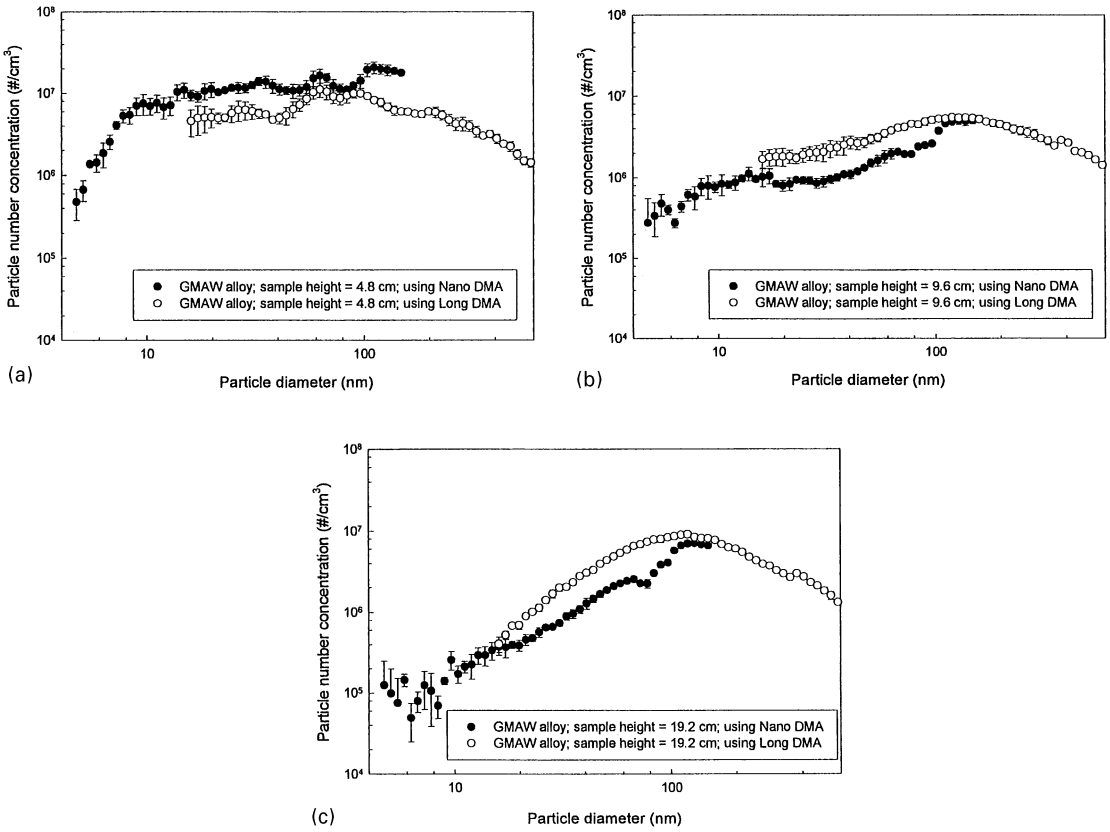

Fig. 6. Scanning mobility particle sizer results for a gas metal arc welding (GMAW) alloy: (a) 4.8 cm above the arc centerline, (b) 9.6 cm above the arc centerline, and (c) 19.2 cm above the arc centerline using both a nano DMA (4.53 nm $< d_p <$ 153 nm) and long DMA (16.5 nm $< d_p <$ 562 nm).

correlate well with one another. As the sample height increased to 9.6 cm (corresponding to a residence time of 1.6 s), a substantial decrease in the particle number concentration was noted for particle diameters less than 100 nm (Fig. 6b). In the overlap regions for the nano and long DMA, a mode appears to be evident for both instruments at a particle diameter of approximately 120 nm. At this sample height, both the nano and long DMA results appear to be significantly smoothed when compared to the previous results (Fig. 6a). Both the reduction in the number concentration of small particles and the smoothing of the particle size distribution become more pronounced as the sample height increased further to 19.2 cm (with a corresponding residence time of 3.2 s) (Fig. 6c). For example, when the sample height changed from 4.8 to 19.2 cm, the particle number concentration decreased by 20-fold for particle diameters less than 40 nm.

To observe the aerosol dynamics associated with the temporal evolution of the welding fumes over a longer time-scale, a welding burst experiment was conducted (Fig. 7). In this experiment, the chamber air was HEPA filtered to remove particles from within the chamber (volume $\sim$ 890 l), and the ventilation system was turned off. Welding was conducted over a very short time (2 s) using a GMAW alloy (designated as ER70S-6) and 90% Ar/10% CO_2 shield gas (flowrate of 18 lpm).

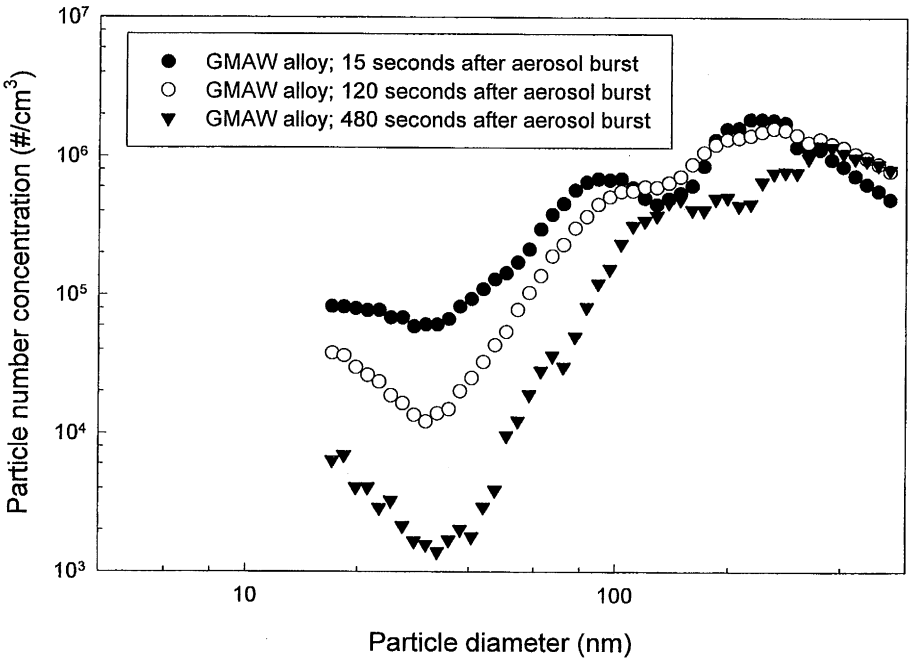

Fig. 7. Scanning mobility particle sizer results as a function of time for a 2 s burst of welding fume into a stagnant chamber using a gas metal arc welding (GMAW) alloy (note: a long DMA was used with 16.5 nm $< d_p <$ 562 nm).

SMPS measurements were taken using the long DMA (16.5 nm $< d_p <$ 562 nm) to determine how the particle size distribution evolved with respect to time. Multiple experimental runs were conducted to insure reproducibility of these results.

The welding aerosols are clearly multi-modal (Fig. 7). For particle diameters less than 40 nm, a 20-fold decrease is noted in the particle number concentration when comparing the initial to final SMPS sample run (a finding that is similar to that of Fig. 6a–c). Again, it appears that coagulation is responsible for scavenging of smaller particles by larger particles. When observing particles in the other modes, the particle diameter increased with increasing time. For example, the SMPS run started at 15 s after the initial welding burst has modes corresponding approximately to 90 and 246 nm. As the aerosol evolved within the chamber, the SMPS run started at 120 s after the welding burst showed that these modes had increased in diameter to 104 and 264 nm, respectively. Interestingly, the SMPS run conducted 480 s after the welding burst showed a further increase in the two modes to particle diameters of 200 and 352 nm, respectively. In addition, a 56% decrease in the total particle number concentration was noted from the initial to the final SMPS run.

The experimental results obtained for the welding burst experiment (Fig. 7) were also compared to the predicted values of a coagulation model (Fig. 8a and b) (Baron, 1994; Park, Lee, Otto, & Fissan, 1999). This model provides an analytical, temporal solution for coagulation over the entire particle size range. Using the particle size distribution statistics for the initial SMPS experimental run, the predicted behavior of the aerosol was plotted over a relatively short time period (Fig. 8a) and compared to the experimental results obtained for the SMPS runs conducted

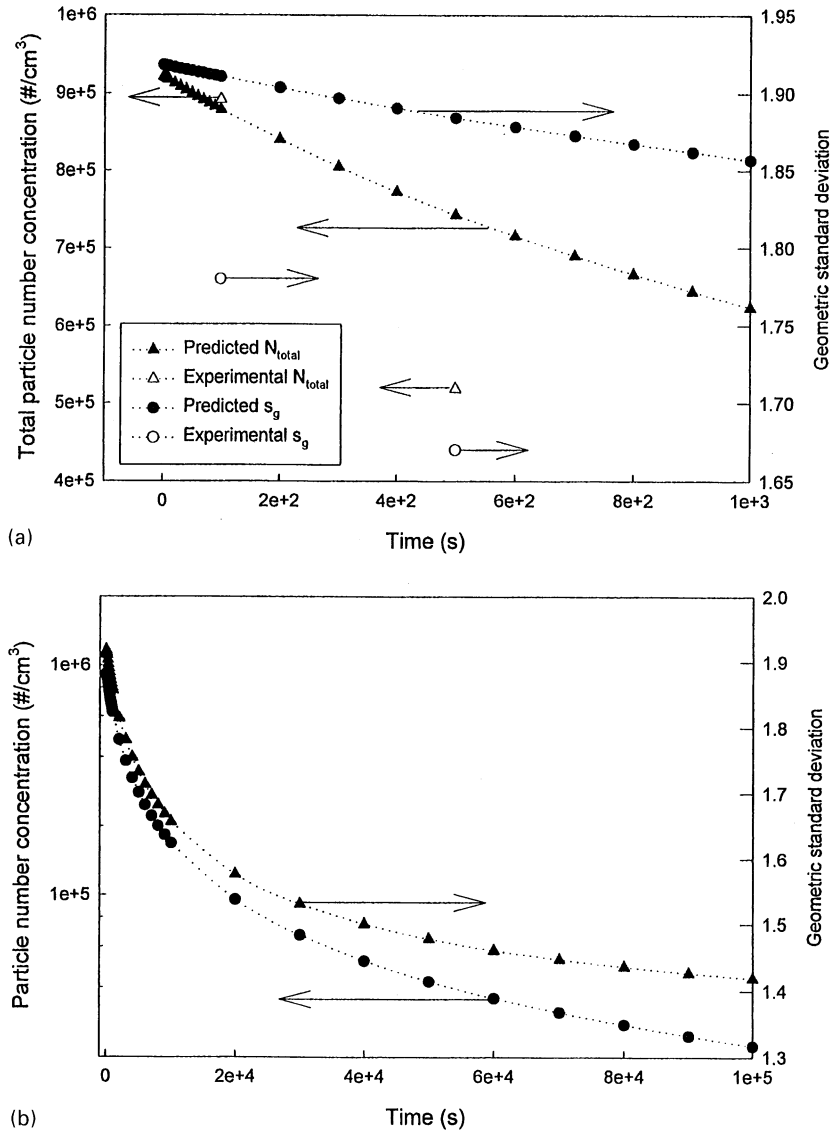

Fig. 8. Predicted and experimental changes in number concentration and geometric standard deviation over: (a) short-time periods, and (b) long-time periods using a coagulation model (Park et al., 1999) and the SMPS data collected during the welding burst experiment (Fig. 2.7).

at 120 and 480 s. At 120 s, the predicted and experimental total number concentration are quite close to one another. At 480 s, the experimental number concentration is about 30% lower than the predicted number concentration. This may be explained as follows. At increasing times, the particle size distribution clearly shifts to larger particle sizes (Fig. 7). Experimentally, the particle size range of the SMPS is no longer obtaining information on the right-hand side of the particle size distribution. Therefore, the measured number concentration of the SMPS would tend to be lower

than the predicted number concentration, especially over long-time periods. Additionally, particle losses to the sides of the chamber would also serve to reduce the measured number concentration.

When observing the experimental and predicted geometric standard deviations, the experimental values are lower than the predicted values for both the 120 and 480 second sample runs. At 120 s the experimental value is seven percent lower than the predicted value (1.78 versus 1.91, respectively). At 480 s, the experimental value is eleven percent lower than the predicted value (1.67 versus 1.88, respectively). Using the same reasoning, the right-hand side of the particle size distribution is no longer being measured. As a result, the SMPS is no longer able to measure the right-hand side of the particle size distribution, resulting in a smaller measured geometric standard deviation. Over time, the variation between the predicted and measured values should increase, and this behavior was noted. Over longer time periods, the coagulation model predicts asymptotic behavior to occur at times greater than 1×10^5 s (Fig. 8b).

Several observations were made in both the flowing and stagnant chamber experiments and include: (1) the reduction in the number concentration of small particles (Figs. 6a–c and 7), (2) the smoothing of the particle size distribution as the sample height increases (Fig. 6a–c), and (3) the shift in the modes of the multi-modal distributions to larger particle sizes (Fig. 7). Coagulation processes can be used to explain the temporal evolution of the welding aerosol. Aerosols will coagulate to form larger particles that result in an overall decrease in the particle number concentration. Additionally, coagulation of smaller particles with larger particles is dynamically favored such that the particles in the nucleation mode will be scavenged by larger particles in the accumulation modes. This will result in the experimentally observed shift in the modes to larger particle diameters.

The multi-modal nature of the welding aerosol (Figs. 6a–c and 7) is thought to be the first time this behavior had been observed. The dynamics of an arc welding process are quite complex (Fig. 1). Welding aerosols are initially formed from the nucleation of vapors emanating from the superheated metal droplets located within the arc, and from spatter particles ejected from the welding process. Chemical kinetics, primarily involving reactions of oxygen with the metal vapors, also serve to increase the complexity of this process and will also play a role in the formation of welding aerosols. Probable explanations for this multi-modal behavior may include: the welding aerosols are composed of chemically distinct metal species, and/or aerosol dynamics of the fumes created from the vapors contained within the arc occur at time-scales that are different from that of the welding spatter. Future work entails collecting size-fractionated aerosol samples near the arc to determine if the modes are chemically/morphologically distinct. The effect of spatter on the dynamics of an arc welding process also needs further investigation, as this mechanism has been shown to significantly contribute to the fume formation rate (Gray, Hewitt, & Hicks, 1980).

4. Conclusions

The design, construction, and validation results of a welding fume generation chamber and aerosol sampling system to characterize welding fumes from an "ultrafine" aerosol perspective was presented. The experimental apparatus was designed to allow for flexibility in changing arc welding parameters, sample locations, and to promote the steady-state generation of fumes over a period of

several minutes. CPC measurements, used to characterize the spatial and temporal behavior of the fume generation apparatus, revealed that the system was well-behaved and yielded reproducible results. Experiments conducted using alloys from two different welding processes (GMAW and FCAW) showed that choice of welding alloy had a marked effect on the particle number size distribution, morphology and chemistry aspects of the resultant fume. SMPS experiments revealed that the particle number size distributions resulting from gas metal arc welding operations were multi-modal and dynamically changed with respect to time. This apparatus represents a significant improvement in characterizing arc welding fumes by allowing ease in changing welding/aerosol sampling parameters, and characterizing the aerosol behavior both spatially and temporally.

References

Baron, P. A. (1994). *Aerosol calculator* (computer spreadsheet). St. Paul, MN: TSI, Inc

Biswas, P., Li, X., & Pratsinis, S. E. (1989). Optical waveguide preform fabrication. *Journal of Applied Physics*, *65*, 2445.

Fasiska, E. J., Nasta, M. A., & Scarr, G. K. (1982). Use of STEM in particulate characterization. *International symposium for testing and failure analysis*, Torrance, CA (pp. 322–327).

Ferin, J., Oberdorster, G., Penney, S., & Soderholm, S. C., Gelein, R., & Piper, H. C. (1990). Increased pulmonary toxicity of ultrafine particles? I. Particle clearance, translocation, morphology. *Journal of Aerosol Science*, *21*, 381–383.

Gilmour, P., Brown, D. M., Beswick, H., & Benton, B., MacNee, W., & Donaldson, K. (1997). Surface free radical activity of PM10 and ultrafine titanium dioxide: a unifying factor in their toxicity? *Annals of Occupational Hygiene*, *41*(Suppl. 1), 32–38.

Gray, C. N., & Hewitt, P. J. (1982). Control of particulate emissions from electric-arc welding by process modification. *Annals of Occupational Hygiene*, *25*, 431–438.

Gray, C. N., Hewitt, P. J., & Hicks, R. (1980). The effect of oxygen on the rate of fume formation in metal inert gas welding arcs. *Weld pool chemistry and metallurgy* (pp. 167–175). London: The Welding Institute.

Heile, R. R., & Hill, D. C. (1975). Particulate fume generation in arc welding processes. *Welding Journal*, *54*, 201s–210s.

Hewett, P. (1995). The particle size distribution, density, and specific surface area of welding fumes from SMAW and GMAW mild and stainless steel consumables. *American Industrial Hygiene Association, Journal*, *56*, 128–135.

Hewitt, P. J., & Gray, C. N. (1983). Some difficulties in the assessment of electrical arc welding fume. *American Industrial Hygiene Association, Journal*, *44*, 727–732.

Hilton, D. E., & Plumridge, P. N. (1991). Particulate fume generation during GMAW and GTAW. *Welding and Metal Fabrication 59*, 555–562.

Hinds, W. C. (1999). *Aerosol technology* (pp. 187–194). New York: Wiley.

Kalliomaki, P. L., Grekula, J., Hagberg, & Sivonen, S. (1987). Analytical electron microscopy of welding fumes. *Journal of Aerosol Science*, *18*, 781–784.

Lin, W. Y., & Biswas, P. (1994). Metallic particle formation and growth dynamics during incineration. *Combustion Science and Technology*, *101*, 29–43.

National Institute for Occupational Safety and Health NIOSH. (1988). *NIOSH Criteria for a recommended standard*: *Welding*, *brazing*, *and thermal cutting* (pp. 88–110). Cincinnati, OH: DHHS, CDC, NIOSH.

Oberdorster, G., Ferin, J., Penney, D. P., Soderholm, S. C., Gelein, R., & Piper, H. C. (1990). Increased pulmonary toxicity of ultrafine particles? II. lung lavage studies. *Journal of Aerosol Science*, *21*, 384–387.

Park, S. H., Lee, K. W., Otto, E., & Fissan, H. (1999). The log-normal size distribution theory of Brownian aerosol coagulation for the entire particle size range: part I — analytical solution using harmonic mean coagulation kernel. *Journal of Aerosol Science*, *30*, 3–16.

Takenaka, S., Dornhofer-Takenaka, H., & Muhle, H. (1986). Aveolar distribution of fly ash and titanium dioxide after long-term inhalation by Wistar rats. *Journal of Aerosol Science*, *17*, 361–364.

Tandon, R. K., Payling, R., Chenhall, B. E., Crisp, P. T., Ellis, J., & Baker, R. S. (1985). Application of X-ray photoelectron spectroscopy to the analysis of stainless-steel welding aerosols. *Applied Surface Science*, *20*, 527–537.

Thornton, M., & Stares, I. (1994). Analysis of particulate fume generation rates from gas metal arc welding. *Welding Review International*, *13*, 363–365.

Ulfvarson, U. (1981). Survey of air contaminants from welding. *Scandanavian Journal of Work and Environmental Health*, *2*, 1–28.

Voitkevich, V. G. (1988). Investigation of the heterogeneity of welding fume particle composition by the method of X-ray photoelectron spectroscopy. *Welding in the World, Le Soudage Dans Le Monde*, *26*, 108–111.